

On the topographical/chemical analysis of polycrystalline diamond pulsed laser ablated surfaces

M. Pacella*, D. A. Axinte, P. W. Butler-Smith, M. Daine

Faculty of Engineering, Department of Mechanical, Materials and Manufacturing Engineering, University of Nottingham, NG7 2RD, UK

* Corresponding author. Tel.: +44(0)1159514063; E-mail address: eaxmp1@nottingham.ac.uk

Abstract

Pulse laser ablation (PLA) is a widely used material removal technique. This paper investigates the effects of various changes of laser parameters on surface integrity and binder composition when PLA (using a Nd: YAG laser) on polycrystalline diamond composites (grain size 2–25 μm , binder Cobalt). Firstly, 2D/3D surface micro-geometry has been evaluated using contact autofocus profiling. Environmental scanning electron microscopy was carried out to establish surface damages after ablation on different grain size composites. Compositional chemical analyses were performed by Energy-dispersive X-ray spectroscopy, to evaluate the role of binder percentage in the surface integrity after ablation. This showed an increased percentage of Cobalt in particular in the areas of higher energy density/fluence. In particular, as a consequence of a single spot laser ablation, the coarse and fine grain composites proved to have similar reaction to laser ablation in term of remaining Co percentage, while in the ablation of a continuous groove the fine diamond grain specimen showed an higher Co percentage than the coarse specimen (35% versus 20%) proving that the percentage of the Cobalt in the ablated area is proportional to the material percentage before laser ablation.

© 2014 The Authors. Published by Elsevier B.V. Open access under [CC BY-NC-ND license](https://creativecommons.org/licenses/by-nc-nd/4.0/).

Selection and peer-review under responsibility of The International Scientific Committee of the “2nd Conference on Surface Integrity” in the person of the Conference Chair Prof Dragos Axinte dragos.axinte@nottingham.ac.uk

Keywords: Laser micro machining - Polycrystalline diamond - Scanning electron microscopy - X-ray spectroscopy

1. Introduction

Polycrystalline diamonds (PCD) are sintered at high pressure and high temperatures conditions to form a solid structure of randomly oriented, intergrown, diamond particles incorporated in a matrix which include a metal catalyst such as Cobalt [1].

In the last decade, the use of diamond in engineering has been increasing because of the highly competitive combination of its properties such as hardness, electrical conductivity and thermal stability. Its hardness (Knoop micro-hardness 48 – 52 *GPa* [2]) made it a very difficult to shape material, and the necessity to find a way of shaping it in a fast and economic way lead researchers to find new technologies. A research conducted in 2001 [3] has shown that the surface smoothness of the structures produced by Pulsed Laser Ablation (PLA) in metals produced a quality standard comparable to the Electric Discharge Milling (EDM). Most recent researches have recognised PLA as an effective and promising technique for surface processing of diamonds. In 2009 laser cutting has been utilised for precise shaping in jewellery

fabrication and for engineering applications such as manufacture of diamond anvils and generation of precise micro-tools [4]. As such, PLA proved its use for surface processing of hard metals and ceramics.

Being PLA a thermal process, involving the material chemical phase (solid/liquid/gaseous) changes within a very short time interval with a minimum thermal affected zone, PLA requires a minimum laser energy density threshold depending on the thermal/optical properties of the target material [5]. In order to enable the morphological control in the generation of freeform surfaces onto the target material two types of parameters are commonly considered during the PLA process:

- Energy parameters such as average laser power (P_m [*W*]) and pulse duration (τ [μs]);
- Kinematics parameters such as laser frequency (f [*kHz*]) and feed speed (v [*mm/s*]).

Hence, the study of the effects of those parameters in PLA of PCD is critical to the generation of surfaces with minimum thermal affected area. Although a wide range of literature has been found on laser machining of brittle

and hard materials, few studies have been conducted on the laser material removal mechanism of polycrystalline diamond composites (PCD), in particular little attention has been given to the variation of binder percentage as a function of energy density and fluence.

Scope of the paper

The present study evaluates the effects of kinematic/energetic parameters in pulsed laser ablation of fine/coarse polycrystalline diamond grain composites by a combined technique of Energy-dispersive X-ray spectroscopy and ESEM microscopy. The study covers the evaluation of five sites of chemical analysis for a single spot and a continuous groove obtained by PLA; each of the five areas corresponds to various radial positions on the laser spot characterised by different energy density/fluencies (as the energy distribution across the beam follows a Gaussian distribution). The parameters effects on the surface integrity of diamond composites are evaluated by:

- topographical morphology at different beam feed speed on coarse/fine grain PCD to evaluate optimised kinematic parameters for PLA;
- microscopical analyses at different laser average power to evaluate the effects of energetic parameters on the ablated composite integrity;
- response of the metallic binder (Cobalt) to the laser ablation process considering its physical phase change and its possible interaction with the diamond grains in case of a coarse grain or a fine grain.

2. Materials and method

In this study, in order to perform three set of experiment, two PCD composites (10x10mm, thickness=1.5mm) were chosen: coarse (PCD CTH025, average grain size 25 μm , Co binder volume circa 8%) and fine (PCD CTC002, average grain size 2 μm , Co binder volume circa 15%) grains polycrystalline diamond specimen depicted in Fig. 1 and Fig. 2 respectively where the higher Co percentage is evident in the bright areas.

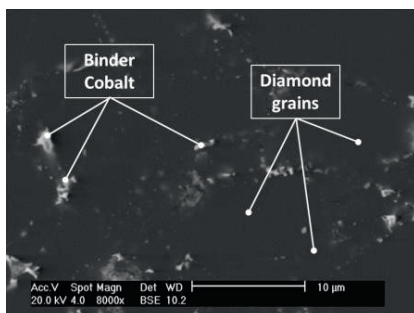


Fig. 1. ESEM backscatter image of a polished diamond grain structure before PLA of a coarse CTH025 grain size diamond (average grain size is 25 μm).

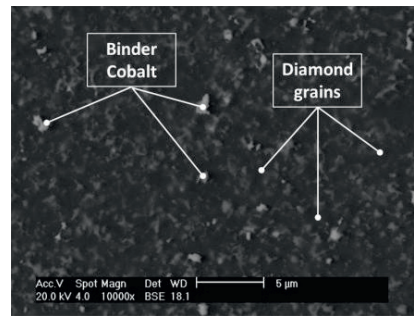


Fig. 2. ESEM backscatter image of a polished diamond grain structure before PLA of a fine CTC002 diamond (average grain size is 2 μm).

This work included three set of experiments: Test 1 was performed to optimize the ablation of single spot/groove as a function of the energetic parameters (P_m 50-100W), Test 2 aimed at optimizing the kinematic parameters in the ablation (v 100-500 mms^{-1}) to obtain, through overlapped spots, continuous grooves; Test 3 was performed to analyze the chemical composition of the ablated surfaces at different laser energy densities/fluencies. A DMG LASERTEC 60 HSC Q-switched Nd: YAG laser (laser spot diameter $d[40\mu\text{m}]$, pulse duration $\tau[10-30\mu\text{s}]$, average laser power $P_m[50-100\text{W}]$, laser frequency $f[10-50\text{kHz}]$ and feed speed $v[100-900\text{mms}^{-1}]$) was used for performing the experiments.

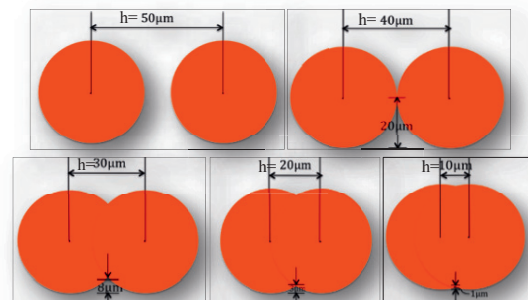


Fig. 3. Schematic representation of Test 2, pulsed laser ablation at different feed speeds: $v=500\text{mms}^{-1}$, $v=400\text{mms}^{-1}$, $v=300\text{mms}^{-1}$, $v=200\text{mms}^{-1}$, $v=100\text{mms}^{-1}$.

The theoretical effects of v on the morphology of the ablated surfaces are shown in Fig.3. A v of 500mms^{-1} was chosen to achieve a single spot ablation; a v of 100mms^{-1} was chosen to reduce the distance between single spot (h [μm]) from 50 μm to 10 μm and to achieve a continuous groove. A Talysurf CSI 1000 contact autofocus profilometer was used for topographical measurements (depth of the spot, volume of ablation) of the ablated areas after Tests 1-2.

A Philips XL30 Environmental Scanning Electron Microscope (ESEM) was used for the evaluation of optimal ablation parameters for Tests 1-2 in term of

thermally affected zone and homogeneity of the spot diameter. Then, the identified optimal parameters (from Tests 1-2) have been used to ablate a single pulse ($P_m 60W, \tau 20\mu s, f 10kHz, v 500mm s^{-1}$) and a continuous groove ($P_m 60W, \tau 20\mu s, f 10kHz, v 100 mm s^{-1}$) onto the composites, preparing the specimens for Test 3 that was aimed at analyzing the chemical composition of the ablated surfaces at various positions across the spot/trench that are characterized by different laser energy densities/fluencies and to evaluate their influence on the local percentage Co binder. For Test 3, the values of laser fluence (F in Jcm^{-2}) and power density (P_L in W) per pulse were calculated using Eq. 1 and 2 [6][7].

$$F_i = \frac{4P_m}{\pi d_i^2 f} \quad i = 1,2..5 \quad (1)$$

$$P_{L_i} = \frac{4P_m}{\pi \tau d_i^2 f} \quad i = 1,2..5 \quad (2)$$

Where d_i [cm] is the radial position on the beam spot diameter which is varying from position 1 to 5 as represented in Fig. 4.

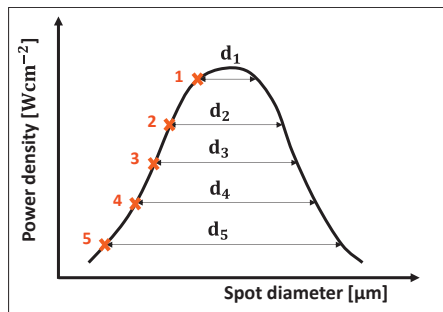


Fig. 4. Schematic representation on a Gaussian of the spot diameter versus the power density; numbers 1 to 5 indicate the areas of EDX analysis corresponding to different radial positions d_i .

As F is dependent on the position across the beam spot (see Eq. 1), five different areas for chemical analysis were chosen on the laser spots/trenches generated on Tests 1 and 2.

3. Results and discussion

Each section of results/discussion corresponds to different analysis technique used for the achievement of the results for the three set of tests.

3.1 Topographical and microscopic analyses on diamond composites when optimising energetic and kinematic PLA parameters.

Numerical results of Test 1 such as calculation of spot depth, ablated areas and ablated volumes are reported in

Table 1, where the values are the average of the two measured values from specimens CTH025-CTC002.

Table 1. Results for specimens CTC002- CTH025 in Test 1.

$P_m(W)$	Depth(μm)	Ablated Area(μm^2)	Ablated Volume(μm^3)
50	5.11	200	1022
60	5.87	161	945
70	6.09	167	1017
80	6.19	202	1250
90	5.10	78.3	399.3
100	3.91	55.8	162.3

Figure 5 represents the topographical footprint of single spot. This is an example of the typical effect of P_m variation on the topography of the PCD. It has been found that for $P_m = 60 W$ (Fig. 5a) a homogeneous spot with well-defined round circumference was achieved; an increase in P_m up to 100W (Fig. 5b) led to a variation of the circumference into a triangular shape with a reduction of spot depth and ablated volume (Table 1).

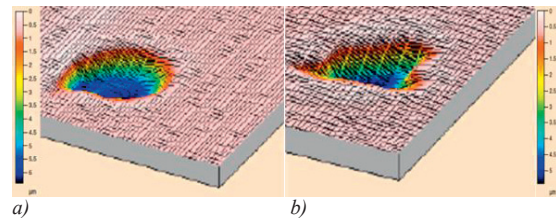


Fig. 5. TALYSURF results of Test 1 for CTC002 for different laser average power: a) P=60W; b) P=100W.

This has been confirmed by microscopical analyses. Examples of ESEM results of Test 1 are shown: fig. 6 shows the typical circular single spot on specimen CTH025 when the surface is ablated at $P_m = 60W$, while Fig. 7 depicts the asymmetrical single spot when P_m is increased to 100W.

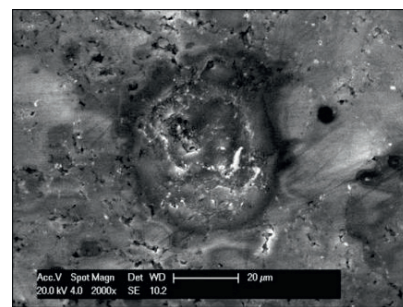


Fig. 6. ESEM imaging of Test 1 for CTH025 for a P_m of 60W.

As previously mentioned an increase of P_m caused a decrease of homogeneity in d , as evident in Figs 6-7. This can be explained considering F : by increasing P_m , equation 1 has shown to give an increase in F . The lack

of homogeneity might arise because the energetic threshold of the target material is exceeded.

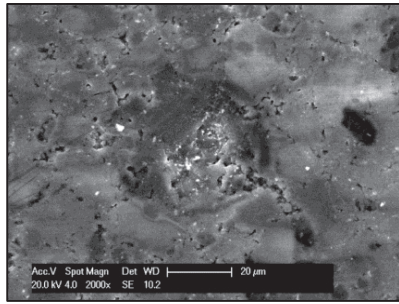


Fig. 7. ESEM imaging of Test 1 for CTH025 for a P_m of 100W.

In fact, when the threshold energy is transferred to the material, ablation takes place, this happens in the case of $P_m = 60W$. With an increased P_m up to 100W, ablation still takes place but there will be remaining energy which the material is able or not to absorb depending on its optical absorbance. This energy is then dissipated in the surrounding area giving rise to the thermally affected zone and producing a lack of homogeneity in the spot circumference. By combining surface topography and ESEM, the optimised P_m for Test 1 was found to be 60W for specimens CTC002-CTH025.

Table 2 contains the parameters used to achieve a single spot (Fig. 8a) and overlapped groove (Fig. 8b), where the column indicating the actual overlapping percentage is achieved averaging the values from CTH025 and CTC002 measured with the profilometer.

Table 2. Parameters and results for Test 2 (actual overlapping is an average of the two materials).

P_m (W)	τ (μ s)	f(kHz)	v (mms ⁻¹)	Actual overlapping (%)
60	20	10	500	0
60	20	10	400	66
60	20	10	300	77
60	20	10	200	90
60	20	10	100	99

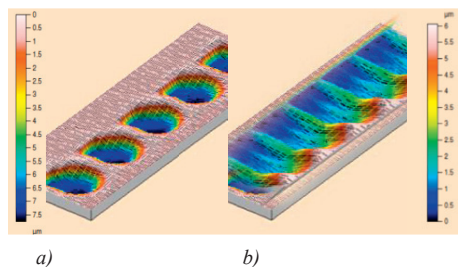


Fig. 8. a) example of the single spot in Test 2 for $v=500mms^{-1}$ b) example of the overlapping spots in Test 2 for $v=300mms^{-1}$.

An example of the topographical profile of specimen CTC002 in Test 2 is reported in Fig. 8 to show the effect of the variation of v on the footprint.

Figure 9 shows a microscopy cross section of Test 2 for specimen CTH025 for the minimum v , 100 mms⁻¹ (Fig. 9b) and maximum v , 500 mms⁻¹ (Fig. 9a).

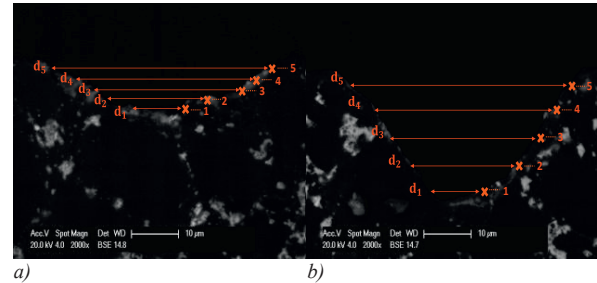


Fig. 9. ESEM imaging of the cross section of the CTH025 specimen showing the areas of analysis of EDX detector for the two different tests: a) optimized single spot from Test 1; b) optimized continuous groove from Test 2.

With the decreased v (from 500mms⁻¹ to 100mms⁻¹), a 30% increase of ablated depth was found; in fact, being v a kinematic parameter, when this has been reduced (and F is kept constant) there is a superimposition of fluencies that continuously overlap each other for every single pulse creating a deeper ablated area and provoking a gap between F of a single spot and F of the continuous groove (those should be constant at the same d_i). Although the only varied parameter is a kinematic one, the topographical/microscopical effect on the ablated area is very similar to the increase in F .

3.2 EDX analysis in test3.

This section focuses specifically on chemical compositional analysis of the single spot and continuous groove ablated composites allowing a complete overview of the laser ablation process both in term of surface integrity and in the chemical analysis of the composites components. Test 3 aimed at comparing the variation of F (in single spot/groove cross section) versus the chemical binder percentage. A P_m of 60 W was chosen as energetic parameter to achieve an ablated single crater (Fig. 9a), while a v of 100 mms⁻¹ was selected as kinematic parameter to achieve an ablated continuous groove (Fig. 9b).

Five areas for EDX analysis were chosen, corresponding to different d_i on the laser spot, which are shown in the cross sections depicted in Fig. 9, with the label 1,2,3,4 and 5. For each of the chosen areas (corresponding to a different d) the calculated values for F and P_L are reported in Table 3: those values are chosen/measured as shown in Fig. 9. The selected areas for EDX analysis are shown in the EDX images in Figs. 10-11, each one corresponding to the diameters reported in Table 3.

Table 3. Values of fluence and power density for the chosen areas.

Area of analysis	$d_i(\mu\text{m})$	$F(\text{Jcm}^{-2})$	$P_L(10^6\text{Wcm}^{-2})$
1	10	7369	382
2	15	3395	169
3	25	1222	61
4	30	849	42
5	35	623	31

The depth of crater resulted from the single spot ablation was found to be 50% smaller than the one resulted from the continuous groove ablation.

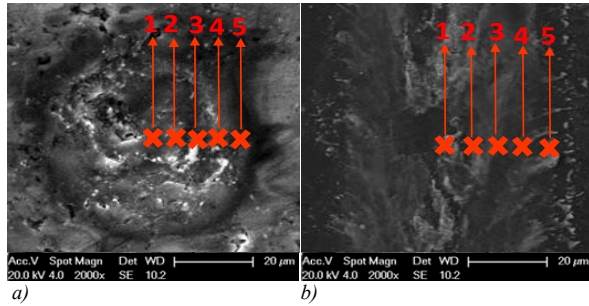


Fig. 10. ESEM imaging showing the EDX areas of analysis for CTH025: a) single spot crater; b) continuous groove.

Chemical analyses conducted on specimens CTH025 (Fig. 10b) have shown that for the area of higher F (Area 1) a higher presence of Co is found (Table 4), while this is decreasing moving towards Area 5, area with lower F . The same result was found for specimen CTC002, where, for higher F the Co percentage was higher than in the low F area (Tables 6-7).

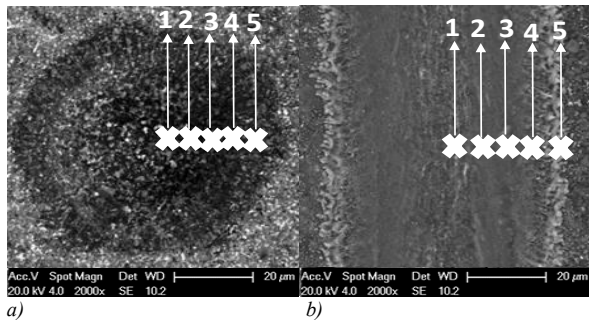


Fig. 11. ESEM imaging showing the EDX areas of analysis for CTC002: a) single spot crater; b) continuous groove.

Preliminary chemical analyses have shown that the initial percentage of Co before pulsed laser ablation is 8% for specimen CTH025 (line blue Fig. 13a-b) and 15% circa for specimen CTC002 (line red Fig. 13a-b). It has been found that after single spot pulsed laser ablation, the Co percentage is higher than the initial 8% in four of the five analysed areas for specimen CTH025 (points 1, 2, 3, 4 above the blue line in Fig. 13a);

whereas the Co percentage is higher only in 2 of the five analysed areas for specimen CTC002 (points 1, 2 above the red line in Fig. 13a).

Table 4. EDX results for the continuous groove ablated in Test 2 ($P_m 60W, \tau 20\mu\text{s}, f 10\text{kHz}, v 100\text{mms}^{-1}$ for CTH025 composite).

Element (%)	C	O	Co
Area 1	66.21	3.77	30.02
Area 2	76.96	-	23.04
Area 3	84.29	-	15.71
Area 4	98.43	-	1.57
Area 5	92.08	5.65	1.48

Table 5. EDX results for the single spot ablated in Test 2 ($P_m 60W, \tau 20\mu\text{s}, f 10\text{kHz}, v 500\text{mms}^{-1}$) for CTH025 composite.

Element (%)	C	O	Co
Area 1	80.73	-	19.27
Area 2	75.99	3.20	17.23
Area 3	81.81	-	16.88
Area 4	86.58	2.67	8.63
Area 5	89.80	3.37	5.14

Table 6. EDX results for the single spot ablated in Test 2 ($P_m 60W, \tau 20\mu\text{s}, f 10\text{kHz}, v 500\text{mms}^{-1}$) for CTC002 composite.

Element (%)	C	O	Co	W
Area 1	50.45	27.40	20.13	2.02
Area 2	79.50	3.29	15.77	1.44
Area 3	74.40	9.68	14.74	1.19
Area 4	81.53	5.49	9.52	3.46
Area 5	62.70	26.98	8.29	2.03

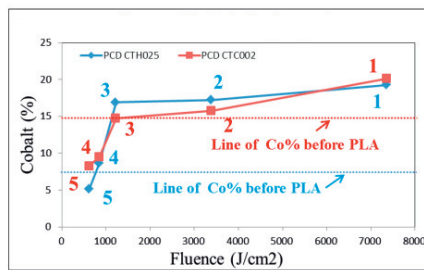
Table 7. EDX results for the groove ablated in Test 2 ($P_m 60W, \tau 20\mu\text{s}, f 10\text{kHz}, v 100\text{mms}^{-1}$) for CTC002 composite.

Element (%)	C	O	Co	W
Area 1	45.96	3.80	38.74	11.50
Area 2	54.58	4.64	36.88	3.90
Area 3	56.29	11.83	27.76	4.11
Area 4	75.71	3.25	17.05	3.99
Area 5	83.19	-	15.70	1.11

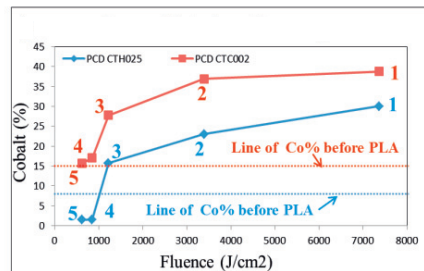
The chemical analyses performed after the continuous groove was ablated have shown that the Co percentage is higher than the initial 8% in three of the five analysed areas for specimen CTH025 (points 1, 2, 3 above the blue line in Fig. 13b); whereas the Co percentage is higher in all of the five analysed areas for specimen CTC002 (points 1, 2, 3, 4, 5 above the red line in Fig. 13b).

In all of the cases it was found that the higher percentage of binder after ablation was corresponding to the areas of higher F . As previously shown in Fig. 4, the representation of the laser beam following a Gaussian distribution, proved to have high F in the area corresponding to the peak of the crater, which is representative of Area 1 for EDX analysis. During PLA, for the higher F , the temperature reached in Area 1 is

higher than the temperature in Area 5 and this resulted in material ablation through vaporization/ sublimation.



a)



b)

Fig. 12. Comparative graphs showing the variation of binder percentage in areas 1 to 5 of specimens CTH025 and CTC002: a) laser ablated single spot; b) laser ablated continuous groove.

4. Conclusion

In this experimental study the effects of energetic and kinematic parameters are investigated and discussed for the pulsed laser ablation of composite polycrystalline diamond target surfaces. The study could be summarised as follows:

1. After pulse laser ablation of a single spot, the difference in binder percentage, evaluated on the beam footprint, between the two specimens decreases. Since the process is fast (feed speed, 500mm s^{-1}), and the fluence is constant in every analysed area, there is no big difference in pulsed laser ablation of fine or coarse polycrystalline diamonds.

2. In the ablation of a continuous groove, the difference in binder percentage between the fine and coarse grain PCD is increased with the laser fluence. In particular, since the speed is at the minimum chosen (100mm s^{-1}) the difference in ablation of fine and coarse grains polycrystalline diamond is evident; the lower speed, by producing overlapping energies in every single spot, provoked an increased fluence causing higher quantity of Cobalt to melt and redeposit.

3. The comparative results of chemical analysis before/after PLA have shown an increased percentage of Cobalt in particular in the areas of highest energy density/fluence. In conclusion, like the fluence, also the laser feed speed proved to make a difference in the laser ablation of fine and coarse grains diamond. By

considering energetic and kinematic thresholds, the reaction of the two specimens have been changing, showing that the coarse grain diamond might be used when prediction of ablation is difficult to achieve prior the process, since the fine grain diamond demonstrated to have a higher Cobalt percentage after ablation due to higher melting/redeposition at overlapped fluencies.

Acknowledgments

The authors would like to acknowledge the support of Element Six for their financial support to the Ph.D. Project as well as Dr. C. Wort, Element Six for his technical assistance on the PCD structures.

References

- [1] M. Pacella, P. W. Butler-Smith, D. A. Axinte, and M. W. Fay, "FIB/TEM/EELS micro/nanometric investigations of the effects of laser ablation on the diamond/binder structure in polycrystalline diamond composites," *J. Mater. Process. Technol.*, Oct. 2013.
- [2] M. W. Cook and P. K. Bossom, "Trends and recent developments in the material manufacture and cutting tool application of polycrystalline diamond and polycrystalline cubic boron nitride," vol. 18, pp. 147–152, 2000.
- [3] P. Heyl, T. Olschewski, and R. W. Wijnaendts, "Manufacturing of 3D structures for micro-tools using laser ablation," *Microelectron. Eng.*, vol. 57–58, pp. 775–780, Sep. 2001.
- [4] H. Ohfujii, T. Okuchi, S. Odake, H. Kagi, H. Sumiya, and T. Irifune, "Micro-/nanostructural investigation of laser-cut surfaces of single- and polycrystalline diamonds," *Diam. Relat. Mater.*, vol. 19, no. 7–9, pp. 1040–1051, Jul. 2010.
- [5] Bauerle, *Laser processing and chemistry*. Springer-Verlag, 2000.
- [6] G. F. Zhang, B. Zhang, Z. H. Deng, and J. F. Chen, "An Experimental Study on Laser Cutting Mechanisms of Polycrystalline Diamond Compacts," *CIRP Ann. - Manuf. Technol.*, vol. 56, no. 1, pp. 201–204, Jan. 2007.
- [7] M. Marcodelucas, L. Lavisse, and G. Pillon, "Microstructural and tribological study of Nd:YAG laser treated titanium plates," *Tribol. Int.*, vol. 41, no. 11, pp. 985–991, Nov. 2008.